Exclusive charm production in $\bar{p}p$ collisions at $\sqrt{s} \lesssim 15$ GeV

A. I. Titov[1,2] and B. Kämpfer[1,3]
[1]*Forschungzentrum Dresden-Rossendorf, D-01314 Dresden, Germany*
[2]*Bogoliubov Laboratory of Theoretical Physics, JINR, RU-141980 Dubna, Russia*
[3]*Institut für Theoretische Physik, TU Dresden, D-01062 Dresden, Germany*
(Received 9 June 2008; published 5 August 2008)

We discuss the open charm production in the peripheral reactions $\bar{p}p \to \bar{Y}_c Y_c$ and $\bar{p}p \to M_c \bar{M}_c$, where Y_c and M_c stand for Λ_c^+, Σ_c^+ and D, D^*, respectively, at $\sqrt{s} \lesssim 15$ GeV, which corresponds to the energy range of FAIR. Our consideration is based on the topological decomposition of the planar quark and diquark diagrams, which allows us to estimate consistently meson and baryon exchange trajectories and energy scale parameters as well. The spin dependance is determined by the effective interaction of the lowest exchanged resonance. Unknown parameters are fixed by an independent analysis of open strangeness production in $\bar{p}p \to \bar{Y}Y$ and $\bar{p}p \to \bar{K}K$ reactions and of SU(4) symmetry. We present the corresponding cross sections and longitudinal double-spin asymmetries for exclusive binary reactions with open charm mesons and baryons in the final state. The polarization observables have a nontrivial t and s dependence that is sensitive to details of the open charm production mechanism.

DOI: 10.1103/PhysRevC.78.025201 PACS number(s): 13.85.−t, 11.80.−m, 11.55.Jy, 25.40.Ve

I. INTRODUCTION

Open charm production will be one of the major topics of the hadron and heavy-ion program at FAIR [1]. Charm spectroscopy will be addressed by the PANDA Collaboration [2], and the CBM Xollaboration [3] will exploit charmed particles as probes of the nuclear medium at maximum compression. For both large-scale experiments at FAIR one needs to know the properties of charmed baryons and mesons as well as their production processes in elementary pp and $\bar{p}p$ reactions. For this the opportunities at FAIR are promising, as, for instance, the PAX Collaboration [4] envisages the use a polarized antiproton beam. This offers the chance to study in depth the mechanism of open charm production at the moderate energies from threshold to $\sqrt{s} \lesssim 15$ GeV. In this energy range the phenomenology of charm production is not well established. In present paper we select one important problem of this wide field, namely, the analysis of exclusive binary reactions $\bar{p}p \to \bar{Y}_c Y_c$, $\bar{p}p \to D\bar{D}$, $\bar{p}p \to D\bar{D}^*$, etc. in peripheral collisions in the mentioned energy range.

Since the initial energy is not asymptotically high, the widely used models for the heavy-quark production based on perturbative QCD (see, e.g., Refs. [5–7]) are not applicable, and an essential improvement by including high-order corrections is needed [8,9]. Another severe problem is related to the dynamics of charm productions. In the popular QCD models, the c quark is produced through gluon fragmentation. For c production in peripheral collisions such a gluon must have a large momentum (large $x \sim 1$), that is, much larger than its average value in a nucleon ($x \lesssim 0.2$), and therefore this mechanism is strongly suppressed.

It is expected that the mechanisms of peripheral charm production in $\bar{p}p \to D\bar{D}$ and $\bar{p}p \to \bar{Y}_c Y_c$ reactions are similar to the strangeness production in $\bar{p}p \to \bar{K}K$ and $\bar{p}p \to \bar{Y}Y$ reactions, respectively, which were described successfully in terms of Regge pole models [10–13] with certain baryon and vector meson exchange trajectories. However, a direct extrapolation of such models to the charm production faces a problem. First, the linear Regge trajectories leads to large negative values of the corresponding intercepts $\alpha_{\Lambda_c}(0) \sim -4.5$ and $\alpha_{D^*}(0) \sim -2$. This would result in a suppression of the charm production in peripheral reactions, which contradicts the corresponding data on inclusive charm production. This means, in turn, that the trajectories connected to masses and spins of the charmed hadrons must be essentially nonlinear (cf. Refs. [14,15]). Another problem is the estimate of the energy scale parameter in the Regge pole propagator, which also strongly affects the cross sections.

Therefore, using a model based essentially on a nonperturbative QCD background would seem to be reliable for describing the peripheral reactions. Such an approach was developed in Refs. [16–18] and applied for the evaluation of cross sections of the exclusive Λ_c production in πp and pp collisions. The binary $\pi^- p \to D^- \Lambda_c$ exclusive process plays an important role in this consideration [17]. The model for this reaction is based on quark-gluon string dynamics, under the assumption of the annihilation of a $q\bar{q}$ pair in the interaction and the formation of a $q\bar{q}$ color tube with subsequent decay to the observed hadrons (see also Refs. [19,20]). Schematically, the process $\pi^- p \to D^- \Lambda_c$ is described by the planar diagram shown in Fig. 1(a). A more general case is exhibited in Fig. 1(b). The assumption of the formation and decay of color-gluon strings allows us to construct the space-time evolution of the process and to obtain the factorization condition, where the imaginary part of the amplitude of the process $ab \to cd$ is expressed via a product of the probabilities w_{ab} and w_{cd} of the elastic scattering of $ab \to ab$ and $cd \to cd$, respectively. This gives a consistent prescription for evaluating the parameters of the amplitude (trajectories and energy scale parameters) of the nondiagonal transition $ab \to cd$.

The aim of the present paper is to extend the results of Refs. [16–18] for exclusive charm production in $\bar{p}p$ collisions. In our consideration we analyze simultaneously the open

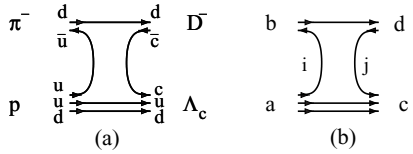

FIG. 1. Diagrammatic representation of the planar diagram for the reaction $\pi^- p \to D^- \Lambda_c$ (a) and for the more general case (b).

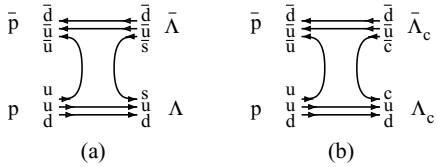

FIG. 2. Planar diagram for the reactions $\bar{p} \to \Lambda\Lambda$ (a) and $\bar{p} \to \Lambda_c\Lambda_c$ (b).

charm and open strangeness production. We are going to consider the reactions $\bar{p}p \to \bar{\Lambda}\Lambda$ and $\bar{p}p \to \bar{\Lambda}_c\Lambda_c$, $\bar{p}p \to \bar{K}K$, and $\bar{p}p \to D\bar{D}$, etc. The strangeness production is of interest in its own right, but some available (although relatively old) experimental data allow us to fix the unknown parameters of the model and get absolute values of the cross sections of the open charm production. We also analyze the double longitudinal asymmetry, which will be accessible in the FAIR PAX experiment with the polarized antiproton beam. The spin dependence of the amplitudes is generated by the symmetry of the PNY and VNY interactions ($P = K, D$ and $V = K^*, D^*, \ldots$), which was widely used in various studies (see, e.g., Refs. [21,22]).

For completeness, we mention that some aspects of the inclusive charm production in terms of the quark-gluon string model were discussed in Refs. [23,24], polarization effects in open charm photoproduction were considered in Ref. [25], propagation of charmed hadrons in the nuclear medium were analyzed in Refs. [26–28], and open charm production in relativistic nucleus-nucleus collisions over a wide energy region was analyzed in Ref. [29].

Our paper is organized as follows. In Sec. II we analyze the strangeness production in the reactions $\bar{p}p \to \bar{\Lambda}\Lambda$, $\bar{p}p \to \bar{\Lambda}\Sigma^0$, and $\bar{p}p \to \bar{\Sigma}^0\Sigma^0$, and the open charm production in $\bar{p}p \to \bar{\Lambda}_c^+\Lambda_c^+$, $\bar{p}p \to \bar{\Lambda}_c^+\Sigma_c^+$, and $\bar{p}p \to \bar{\Sigma}_c^+\Sigma_c^+$ processes, where the dominant contribution comes from the K^* and D^* exchange trajectories, respectively. First, we note equations for the invariant amplitudes and then discuss our results for the differential cross sections and the longitudinal asymmetry. In Sec. III we provide a similar analysis for the $\bar{p}p \to \bar{K}K$ and $\bar{p}p \to D\bar{D}$ reactions, assuming the dominance of strange and charmed baryon exchange trajectories. The reactions $\bar{p}p \to \bar{K}K^*$ and $\bar{p}p \to D\bar{D}^*$ are discussed in Sec. IV. The summary is given in Sec. V.

II. REACTIONS $\bar{p}p \to \bar{Y}Y$ AND $\bar{p}p \to \bar{Y}_c Y_c'$

In this section, we discuss strange and charmed baryon-antibaryon production in peripheral $\bar{p}p$ collisions. For the sake of simplicity, we consider the exclusive production of $\bar{\Lambda}\Lambda$ and $\bar{\Lambda}_c\Lambda_c$ pairs. The generalization for reactions with $\bar{\Lambda}\Sigma$, $\bar{\Sigma}\Lambda$, and $\bar{\Sigma}\Sigma$ final states may be done in a straightforward manner.

The corresponding planar diagrams for $\bar{\Lambda}\Lambda$ and $\bar{\Lambda}_c\Lambda_c$ are depicted in Figs. 2(a) and 2(b).

A. Reaction $\bar{p}p \to \bar{\Lambda}\Lambda$

Following Ref. [17] we assume that the amplitude of the reaction $\bar{p}p \to \bar{\Lambda}\Lambda$ has the form of a Regge pole amplitude, dominated by the K^* exchange trajectory:

$$T^{\bar{p}p\to\bar{\Lambda}\Lambda}_{m_f n_f; m_i, n_i} = C(t)\mathcal{M}^{\bar{p}p\to\bar{\Lambda}\Lambda}_{m_f n_f; m_i, n_i}(s,t)\frac{g^2_{K^*N\Lambda}}{s_0} \times \Gamma[1-\alpha_{\bar{s}q}(t)]\left(-\frac{s}{s_{\bar{p}p:\bar{\Lambda}\Lambda}}\right)^{\alpha_{\bar{s}q}(t)-1}, \quad (1)$$

where m_i, m_f, n_i, and n_f are the spin projections of p, Λ, $\bar{p}$, and $\bar{\Lambda}$, respectively, q stands for u and d quarks, $\alpha_{\bar{s}q}(t)$ is the K^{*+} trajectory, $g^2_{K^*N\Lambda}$ is the coupling constant of the $K^*N\Lambda$ interaction, and $s_0 = 1$ GeV is an universal scale parameter. The spin dependence is accumulated in the amplitude $\mathcal{M}$, which is a smooth function of the Mandelstam variables s and t. In the limit of $s \to \infty$ one has $\mathcal{M} \propto s$. The explicit form of $\mathcal{M}$ will be defined later on. The overall residual function $C(t)$ will be found from a comparison with available experimental data.

In our consideration we use the nonlinear representation for the meson trajectories developed in Ref. [15],

$$\alpha(t) = \alpha(0) + \gamma(\sqrt{T} - \sqrt{T-t}), \quad (2)$$

where $\gamma = 3.65\ \text{GeV}^{-1}$ is the universal parameter (a universal slope in the asymptotic region) and $T \gg 1\ \text{GeV}^2$ is the scale parameter, being special for each trajectory. In the diffractive region with $-t \ll T$, the linear approximation

$$\alpha(t) = \alpha(0) + \alpha' t \quad (3)$$

is valid with $\alpha' = \gamma/2\sqrt{T}$.

The intercept $\alpha_{\bar{s}q}(0)$ and the slope $\alpha'_{\bar{s}q}$ of the trajectory for the nondiagonal transition are related to the corresponding parameters for diagonal transitions as follows [15,16]:

$$2\alpha_{\bar{s}q}(0) = \alpha_{\bar{q}q}(0) + \alpha_{\bar{s}s}(0), \quad (4)$$

$$2/\alpha'_{\bar{s}q} = 1/\alpha'_{\bar{q}q} + 1/\alpha'_{\bar{s}s}, \quad (5)$$

where $\alpha_{\bar{q}q}(t)$ and $\alpha_{\bar{s}s}(t)$ are the ρ and ϕ meson trajectories, respectively.

In our numerical calculations we employ

$$\begin{aligned} &\alpha_\rho(0) = 0.55, \quad \sqrt{T_\rho} = 2.46\,\text{GeV}, \quad \alpha'_\rho \simeq 0.742\,\text{GeV}^{-2}, \\ &\alpha_{K^*}(0) = 0.414, \quad \sqrt{T_{K^*}} = 2.58\,\text{GeV}, \quad \alpha'_{K^*} \simeq 0.71\,\text{GeV}^{-2}, \\ &\alpha_\phi(0) = 0.28, \quad \sqrt{T_\phi} \simeq 2.70\,\text{GeV}, \quad \alpha'_\phi \simeq 0.676\,\text{GeV}^{-2}, \end{aligned} \quad (6)$$

where the ρ and K^* trajectories are taken as input according to Ref. [15].

The energy scale parameter $s_{\bar{p}p:\bar{\Lambda}\Lambda}$ in Eq. (1) is related to the corresponding scale parameters for the diagonal transitions $\bar{p}p \to \bar{p}p$, $(s_{\bar{p}p})$ and $\bar{\Lambda}\Lambda \to \bar{\Lambda}\Lambda$, $(s_{\bar{\Lambda}\Lambda})$ as

$$(s_{\bar{p}p:\bar{\Lambda}\Lambda})^{2(\alpha_{K^*}(0)-1)} = (s_{\bar{p}p})^{\alpha_\rho(0)-1} \times (s_{\bar{\Lambda}\Lambda})^{\alpha_\phi(0)-1}. \quad (7)$$

The scale parameter for the diagonal transition s_{ab} is determined by the sum of the transversal masses of the constituent quarks [17],

$$s_{ab} = \left(\sum_i^{n_a} M_{i\perp}\right)\left(\sum_j^{n_b} M_{j\perp}\right), \tag{8}$$

with $M_{q\perp} \simeq 0.5$ GeV, $M_{s\perp} \simeq 0.6$ GeV, and $M_{c\perp} \simeq 1.6$ GeV. This leads to the following values for the scale factors: $s_{\bar{p}p} \simeq 2.25\ \text{GeV}^2$, $s_{\bar{\Lambda}\Lambda} \simeq 2.56\ \text{GeV}^2$, and $s_{\bar{p}p:\bar{\Lambda}\Lambda} \simeq 2.43\ \text{GeV}^2$.

We assume that the spin dependence of the amplitude in Eq. (1) is determined by the symmetry of the $N\Lambda K^*$ interaction given by the effective Lagrangian in the conventional form

$$\mathcal{L}_{K^*NY} = -\bar{Y}\left(\gamma_\mu - \frac{\kappa_{K^*NY}}{M_N + M_Y}\sigma_{\mu\nu}\right) N\partial^\nu K^{*\mu} + \text{h.c.}, \tag{9}$$

where N, Y, and K^* denote the nucleon, hyperon, and the K^* meson fields, respectively, Y stands for Λ, Σ, etc., and κ is the tensor coupling strength, and h.c. stands for hermition conjugate.

Using this form, one can get the amplitude $\mathcal{M}$ in Eq. (1) as

$$\mathcal{M}^{\bar{p}p\to\bar{\Lambda}\Lambda}_{m_f n_f; m_i n_f}(s,t) = \mathcal{N}(s,t)\,\Gamma^{(p)\,\mu}_{m_f m_i}\;\Gamma^{(\bar{p})\,\nu}_{n_f n_i}\left(-g_{\mu\nu} + \frac{q_\mu q_\nu}{q^2}\right), \tag{10}$$

where q's are momentum transfers in the $p\Lambda K^*$ vertex: $q = p_p - p_\Lambda$, with p_p and p_Λ as four-momenta of the incoming proton and outgoing Λ. The functions $\Gamma^{(p,\bar{p})}$ read

$$\begin{aligned}\Gamma^{(p)}_\mu &= \bar{u}_\Lambda\left[(1+\kappa_{K^*N\Lambda})\gamma_\mu - \kappa_{K^*N\Lambda}\frac{(p_p+p_\Lambda)_\mu}{M_N+M_\Lambda}\right]u_p,\\ \Gamma^{(\bar{p})}_\mu &= \bar{v}_{\bar{p}}\left[(1+\kappa_{K^*N\Lambda})\gamma_\mu + \kappa_{K^*N\Lambda}\frac{(p_{\bar{p}}+p_{\bar{\Lambda}})_\mu}{M_N+M_\Lambda}\right]v_{\bar{\Lambda}}.\end{aligned} \tag{11}$$

The normalization factor $\mathcal{N}(s,t)$ eliminates the additional s and t dependence provided by the Dirac structure in Eq. (10), which is beyond the Regge parametrization:

$$\begin{aligned}\mathcal{N}(s,t) &= \frac{F_\infty(s)}{F(s,t)}, \quad F_\infty(s) = 2s,\\ F^2(s,t) &= \text{Tr}(\Gamma^{(p)\,\mu}\Gamma^{(p)\,\mu'\dagger})\text{Tr}(\Gamma^{(\bar{p})\,\nu}\Gamma^{(\bar{p})\,\nu'\dagger})\\ &\quad\times\left(g_{\mu\nu} - \frac{q_\mu q_\nu}{q^2}\right)\left(g_{\mu'\nu'} - \frac{q_{\mu'}q_{\nu'}}{q^2}\right).\end{aligned} \tag{12}$$

For the NYK^* coupling constants we use the average values of the Nijmegen potential [30]: $g_{K^*NY} = -5.18$, $\kappa_{K^*NY} = 2.79$ for $Y = \Lambda$ and $(-3.29, -0.91)$ for $Y = \Sigma^0$.

The cross section is related to the invariant amplitude of Eq. (1) as

$$\frac{d\sigma}{dt} = \frac{1}{16\pi\left(s - 4M_N^2\right)^2}|T_{fi}|^2, \tag{13}$$

where summing and averaging over the spin projection in initial and the final state is provided. We will also discuss the longitudinal double spin asymmetry, defined as

$$\mathcal{A} = \frac{d\sigma^{\leftrightarrows} - d\sigma^{\rightrightarrows}}{d\sigma^{\leftrightarrows} + d\sigma^{\rightrightarrows}}, \tag{14}$$

where the symbols $\leftrightarrows$ and $\rightrightarrows$ correspond to the antiparallel and parallel spin projections of incoming p and $\bar{p}$ with respect to the quantization axis chosen along the proton momentum in the center-of-mass system (c.m.s.).

The generalization for the reactions $\bar{p}p \to \bar{\Lambda}\Sigma$, $\bar{p}p \to \bar{\Sigma}\Lambda$, and $\bar{p}p \to \bar{\Sigma}\Sigma$ is accomplished by the substitutions $M_\Lambda \to M_\Sigma$, $g_{K^*N\Lambda} \to g_{K^*N\Sigma}$, and $\kappa_{K^*N\Lambda} \to \kappa_{K^*N\Sigma}$ in Eqs. (1) and (11).

B. Reaction $\bar{p}p \to \bar{\Lambda}_c\Lambda_c$

In this case, the amplitude is defined by Eq. (1) with the obvious substitutions $\Lambda \to \Lambda_c^+ \equiv \Lambda_c$, $\Sigma^0 \to \Sigma_c^+ \equiv \Sigma_c$, $K^* \to \bar{D}^*$, $\alpha_\phi \to \alpha_{J/\psi}$, etc. As a first approximation, we assume the validity of SU(4) symmetry and, therefore, the coupling constants of the D^*NY_c interaction are chosen to be the same as for the case of K^*NY interaction. The corresponding trajectory and the energy scale parameters read

$$\begin{aligned}\alpha_{D^*}(0) &= -1.02, \quad \sqrt{T_{D^*}} = 3.91\,\text{GeV},\\ \alpha'_{D^*} &\simeq 0.467\,\text{GeV}^{-2}, \quad \alpha_{J/\psi}(0) = -2.60,\\ \sqrt{T_{J/\psi}} &\simeq 5.36\,\text{GeV}, \quad \alpha'_{J/\psi} \simeq 0.34\,\text{GeV}^{-2},\\ s_{\bar{p}p:\bar{\Lambda}_c\Lambda_c} &\simeq 5.98\,\text{GeV}^2.\end{aligned} \tag{15}$$

C. Results

1. *Differential cross sections*

Consider first the strange hyperon production $\bar{p}p \to \bar{Y}Y$, which we use to fix the residual factor $C(t)$ in Eq. (1). In Fig. 3 we show the differential cross section of the reaction $\bar{p}p \to \bar{\Lambda}\Lambda$ and $\bar{p}p \to \bar{\Lambda}\Sigma^0$ as a function of the momentum transfer $t = (p_p - p_Y)^2$ at the initial momentum $p_L = 6$ GeV/c together with the available experimental data [31]. The overall residual factor

$$C(t) = \frac{0.37}{(1 - t/1.15)^2} \tag{16}$$

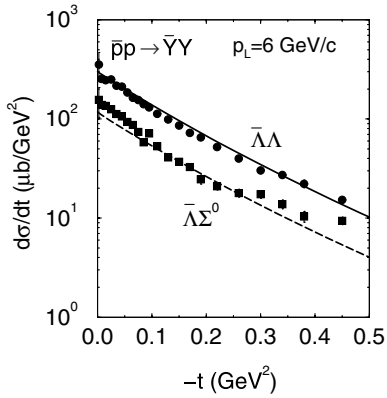

FIG. 3. Differential cross section of the reactions $\bar{p}p \to \bar{\Lambda}$ (solid curve) and $\bar{p}p \to \bar{\Lambda}\Sigma^0$ (dashed curve) as a function of the momentum transfer t at $p_L = 6$ GeV. The experimental data are taken from Ref. [31].

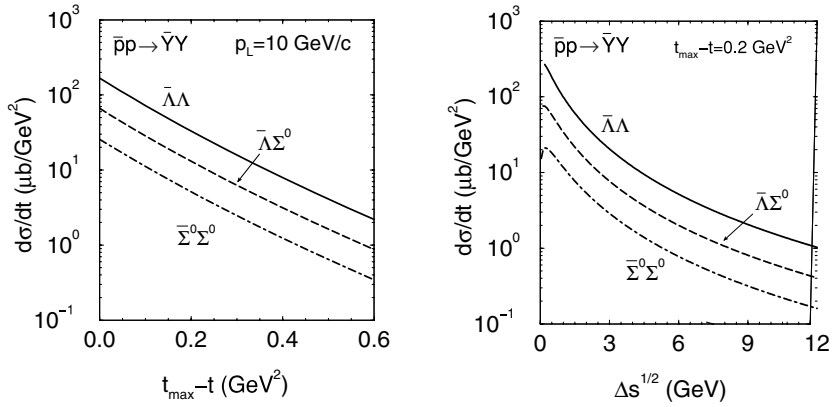

FIG. 4. Left panel: The differential cross sections of the reactions $\bar{p}p \to \bar{\Lambda}\Lambda$ (solid curve), $\bar{p}p \to \bar{\Lambda}\Sigma^0$ (dashed curve), and $\bar{p}p \to \bar{\Sigma}^0\Sigma^0$ (dot-dashed curve) as a function of $t_{\max} - t$ at $p_L = 10$ GeV/c. Right panel: The differential cross section as a function of the excess energy $\Delta s^{1/2}$ at $t_{\max} - t = 0.2$ GeV^2.

provides a reasonable agreement of the calculation and the data.

In Fig. 4 (left panel) we exhibit our prediction for the differential cross sections of the reactions $\bar{p}p \to \bar{\Lambda}\Lambda$, $\bar{p}p \to \bar{\Lambda}\Sigma^0\,(\bar{\Sigma}^0\Lambda)$, and $\bar{p}p \to \bar{\Sigma}^0\Sigma^0$ as a function of $t_{\max} - t$ at initial momentum $p_L = 10\,\text{GeV}/c$. Here, $t_{\max}$ is the maximum momentum transfer, which corresponds to Λ production at zero angle relative to the momentum of the incoming proton in the c.m.s.

The exponential decrease of the cross section is defined by the Regge propagator $(s/s_i)^{2\alpha_{K^*}(t)}$ and the residual $C(t)$. The dependence on the excess energy $\Delta s^{1/2} \equiv \sqrt{s} - \sqrt{s_0}$, where $\sqrt{s_0} = M_{Y'} + M_{\bar{Y}}$, is shown in Fig. 4 (right panel). The calculation is done at fixed $t_{\max} - t = 0.2$ GeV^2. At high energies, the cross section behaves as $s^{2(\alpha_{K^*}-1)} \simeq s^{-1.172}$. The ratio of the cross sections with $\bar{\Lambda}\Lambda$, $\bar{\Lambda}\Sigma^0$, and $\bar{\Sigma}^0\Sigma^0$ final states at high energy reads

$$1 : r : r^2, \tag{17}$$

where $r = (g_{K^*N\Lambda}/g_{K^*N\Sigma})^{-2} \simeq 0.4$.

The predicted differential cross sections of the charm hyperon production are exhibited in Fig. 5. Here, we use the notation $\Lambda_c \equiv \Lambda_c^+$ and $\Sigma_c \equiv \Sigma_c^+$. The left panel shows the dependence on $t_{\max} - t$ at fixed $p_L = 15$ GeV/c. The right panel exhibits the dependence on the energy excess $\Delta s^{1/2}$ at fixed $t_{\max} - t = 0.2$ GeV^2. The threshold initial momenta (for a fixed target) for reactions with $\bar{\Lambda}_c\Lambda_c$, $\bar{\Lambda}_c\Sigma_c$, and $\bar{\Sigma}_c\Sigma_c$ final states are 10.15, 11.83, and 10.85 (GeV/c), respectively. The energy excesses at $p_L = 15$ GeV/c for these final states are 0.90, 0.571, and 0.570 GeV, respectively. This energy is not asymptotically high and some particular behavior of the cross sections in the preasymptotic region is expected. Thus, in Fig. 5 (right panel) one can see a bumplike behavior at low Δs, which reflects the energy dependence of $t_{\max}$ in this region.

2. *Longitudinal asymmetries*

For a better understanding of the results of our numerical calculation, it seems to be useful to perform a qualitative analysis of the longitudinal asymmetry at forward production angle (or $t = t_{\max}$), where the orbital interaction is absent. In this case, the amplitude of the $\bar{p}p \to \bar{Y}Y$ reaction may be written as

$$T_{m_f n_f; m_i, n_i} \sim R(s)\Big(A(s)\,\delta_{m_i m_f}\,\delta_{n_i n_f} + \frac{1}{\sqrt{2}} B(s)\,(1 - 4m_i m_f)\,\delta_{-m_i m_f}\,\delta_{-n_i n_f}\Big), \tag{18}$$

where $R(s)$ is a spin-independent function and m_i, m_f, n_i, and n_f stand for the spin projections of p, Y, $\bar{p}$, and $\bar{Y}$, respectively, The longitudinal asymmetry is expressed through the spin-conserving $[A(s)]$ and spin-flip $[B(s)]$ amplitudes as

$$\mathcal{A} = \frac{B^2(s)}{A^2(s) + B^2(s)}. \tag{19}$$

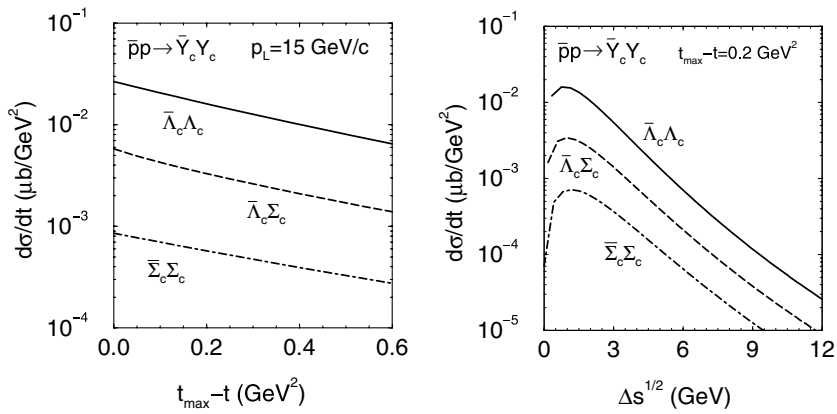

FIG. 5. Left panel: The differential cross sections of the reactions $\bar{p}p \to \bar{\Lambda}_c\Lambda_c$ (solid curve), $\bar{p}p \to \bar{\Lambda}_c\Sigma_c$ (dashed curve), and $\bar{p}p \to \bar{\Sigma}_c\Sigma_c$ (dot-dashed curve) as a function of $t_{\max} - t$ at $p_L = 15$ GeV/c. Right panel: The differential cross section as a function of the excess energy $\Delta s^{1/2}$ at $t_{\max} - t = 0.2$ GeV^2.

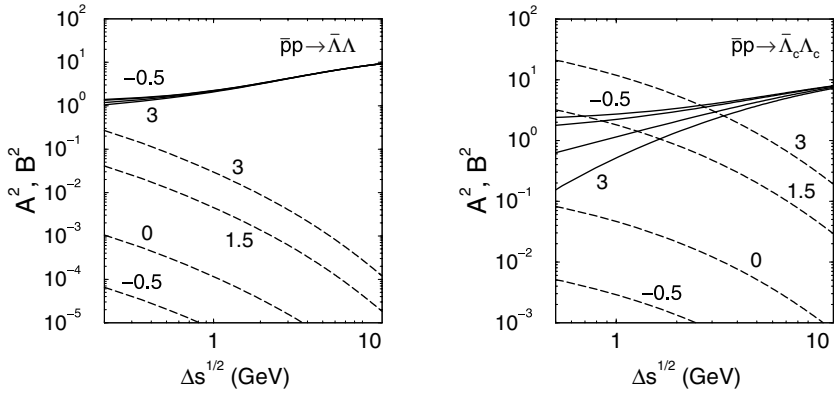

FIG. 6. The quantities A^2 (spin-conserving amplitudes; solid curves) and B^2 (spin-flip amplitudes; dashed curves) as a function of the excess energy $\Delta s^{1/2}$ with $t = t_{\max}$ at different values of the tensor coupling κ. The left and right panels correspond to the reactions $\bar{p}p \to \bar{\Lambda}\Lambda$ and $\bar{p}p \to \bar{\Lambda}_c\Lambda_c$, respectively.

The spin-conserving amplitude is determined by the two functions $a_0(s)$ and $a_\kappa(s)$:

$$A(s) = [a_0(s) + a_\kappa(s)]^2,$$
$$a_0(s) = 1 + \frac{\mathbf{p}_p \mathbf{p}_Y}{(E + M_N)(E + M_Y)},$$
$$a_\kappa(s) = \kappa\, a_0(s) - \frac{2\kappa E}{M_N + M_Y}\left(1 - \frac{\mathbf{p}_p \mathbf{p}_Y}{(E + M_N)(E + M_Y)}\right), \tag{20}$$

where κ is again the tensor coupling strength, $\mathbf{p}_p$ and $\mathbf{p}_Y$ denote the three-momenta of the proton and the outgoing hyperon, respectively, and $E = \sqrt{s}/2$ is the proton energy in the c.m.s. In the case when $M_p \simeq M_Y$ or/and at high energies, when $\sqrt{s} \gg M_Y, a_\kappa \to 0$ and the spin-conserving amplitude becomes independent of κ.

In contrast, the spin-flip amplitude is proportional to the square of the magnetic strength $(1 + \kappa)^2$:

$$B(s) = -\sqrt{2}\left[(1 + \kappa)\left(\frac{\mathbf{p}_p}{E + M_N} - \frac{\mathbf{p}_Y}{E + M_Y}\right)\right]^2. \tag{21}$$

At high energies with $E \gg M_Y$ and $\mathbf{p}_p \simeq \mathbf{p}_Y$, $B(s) \to 0$ and, therefore, the asymmetry in Eq. (19) vanishes. However, at finite energies and large values of $(1 + \kappa)$, the amplitudes $A(s)$ and $B(s)$ are comparable, and the longitudinal asymmetry may be finite and large. The energy dependence of $A^2(s)$ and $B^2(s)$ for the reactions $\bar{p}p \to \bar{\Lambda}\Lambda$ and $\bar{p}p \to \bar{\Lambda}_c\Lambda_c$ is shown in Fig. 6. In the $\bar{\Lambda}\Lambda$ final state, the function $B^2(s)$ is rather small owing to the small difference between M_N and M_Λ. The dependence of $A^2(s)$ on the tensor coupling κ is rather weak. This leads to the small value of the longitudinal asymmetry for the $\bar{p}p \to \bar{\Lambda}\Lambda$ reaction.

In case of the $\bar{p}p \to \bar{\Lambda}_c\Lambda_c$ reaction, the situation is quite different. The large difference between M_N and M_{Λ_c} leads to a large value of $B^2(s)$, shown in Fig. 6 (right panel), and results in a large value of the longitudinal asymmetry.

For the $\bar{p}p \to \bar{\Lambda}\Sigma\,(\bar{\Sigma}\Sigma)$ reactions the spin-flip amplitude $|B(s)|$ is small because of the small magnetic strength, $1 + \kappa \simeq 0.09$, and the asymmetry is almost zero.

Our predictions for the $\bar{p}p \to \bar{Y}Y$ reaction are shown in Fig. 7. The left panel exhibits the t dependence at the initial momentum $p_L = 10$ GeV/c. The right panel shows the dependence on the energy excess at $t_{\max} - t = 0.2$ GeV^2. One can see that the result of the numerical calculations agrees with our qualitative consideration. Thus, for $\bar{p}p \to \bar{\Lambda}\Lambda$, the asymmetry does not exceed 0.2 at forward angles and decreases with energy. In the $\bar{p}p \to \bar{\Lambda}\Sigma$ and $\bar{\Sigma}\Sigma$ reactions it is almost zero.

The longitudinal asymmetry for the $\bar{p}p \to \bar{Y}_c Y_c$ reactions is presented in Fig. 8. In the case of the $\bar{p}p \to \bar{\Lambda}_c\Lambda_c$ reaction, the asymmetry is large at low energy excess and decreases rapidly with energy. In the reactions $\bar{p}p \to \bar{\Lambda}_c\Sigma_c$ and $\bar{\Sigma}_c\Sigma_c$ the asymmetry is negligibly small.

III. REACTION $\bar{p}p \to \bar{M}M$

In this section, we discuss the production of $\bar{M}M$ (with $\bar{M}M$ being $\bar{K}K$ or $D\bar{D}$) in $\bar{p}p$ collisions. We assume that at small momentum transfer $-t$, where $t = (p_p - p_K)^2$ or $t = (p_p - p_{\bar{D}})^2$, the dominant contribution comes from the baryon exchange channels.

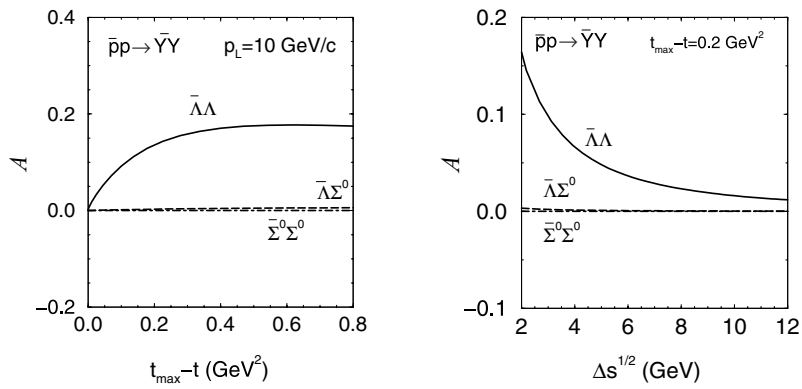

FIG. 7. Left panel: The longitudinal asymmetry for the reactions $\bar{p}p \to \bar{\Lambda}\Lambda$, $\bar{\Lambda}\Sigma^0$, and $\bar{\Sigma}^0\Sigma^0$ as a function of momentum transfer t at $p_L = 10$ GeV. Right panel: The asymmetry as a function of the excess energy at $t_{\max} - t = 0.2$ GeV^2.

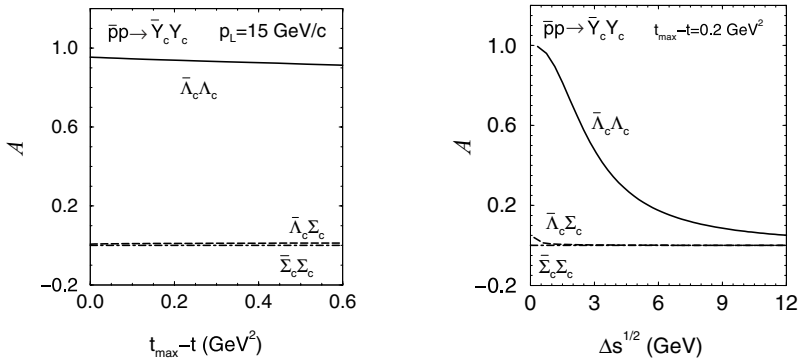

FIG. 8. Left panel: The longitudinal asymmetry for the reactions $\bar{p}p \to \bar{\Lambda}\Lambda$, $\bar{\Lambda}\Sigma^0$, and $\bar{\Lambda}^0\Sigma^0$ as a function of momentum transfer t at $p_L = 10$ GeV. Right panel: The asymmetry as a function of the excess energy at $t_{\max} - t = 0.2$ GeV^2.

As an example, in Figs. 9(a) and 9(b) we show the planar diagrams for $\bar{p}p \to K^-K^+$ and $\bar{p}p \to D^0\bar{D}^0$, with Λ and Λ_c^+ exchange, respectively. The cases of $\Sigma(\Sigma_c^+)$ exchange, or $\Sigma^+(\Sigma_c^{++})$ exchange for the $\bar{K}K(D^+D^-)$ final state, are similar. Here and further on we employ the quark-diquark identity, used in many phenomenological approaches to QCD [14,32,33]. This means that the exchanged baryon is considered as a quark-diquark string object, shown schematically in Fig. 9(c).

A. Reaction $\bar{p}p \to \bar{K}K$

Let us consider first the reaction $\bar{p}p \to \bar{K}K$. For definiteness, we consider $\bar{p}p \to K^-K^+$ with Λ exchange. The cases of Σ and Σ^+ for $\bar{K}^0K^0$ final states may be executed analogously.

The assumption of the quark-diquark identity allows us to generalize our model developed in the previous section. Namely, we assume that the amplitude of the reaction $\bar{p}p \to K^-K^+$ has the form of a Regge pole amplitude dominated by the $\Lambda + \Sigma$ exchange trajectories. Thus, for the Λ exchange it reads

$$T^{\bar{p}p\to K^-K^+}_{m_i,n_i} = C'(t)\mathcal{M}^{\bar{p}p\to K^-K^+}_{m_i,n_i}(s,t)\frac{g^2_{KN\Lambda}}{s_0}\Gamma\left[\frac{1}{2} - \alpha_{ds}(t)\right] \times \left(-\frac{s}{s_{\bar{p}p:\bar{K}K}}\right)^{\alpha_{ds}(t)-\frac{1}{2}}, \quad (22)$$

where m_i and n_i are the spin projections of p and $\bar{p}$, respectively, d stands for a ud diquark, $\alpha_{ds}(t)$ is the Λ trajectory, $g^2_{KN\Lambda}$ is the coupling constant of the $KN\Lambda$ interaction, and $s_0 = 1$ GeV is a universal scale parameter. The spin dependence is accumulated in the amplitude $\mathcal{M}$, which in the limit of $s \to \infty$ results in $\mathcal{M} \approx \sqrt{s}$. The explicit form of $\mathcal{M}$ will be defined later. The overall residual function $C'(t)$ will be found again from a comparison with available experimental data.

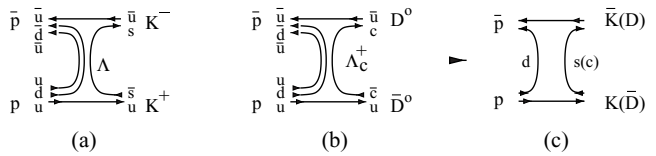

FIG. 9. Planar diagrams for the reactions $\bar{p}p \to K^-K^+$ (a) and $\bar{p}p \to D^0\bar{D}^0$ (b). (c) The exchanged baryon as a quark-diquark object. The symbol d stands for a qq diquark.

The parameters of the trajectory for the nondiagonal transition α_{ds} are related to the corresponding parameters for the "diagonal" transitions $\alpha_{\bar{s}s}$ and $\alpha_{\bar{d}d}$ similarly to Eqs. (4) and (5):

$$2\alpha_{ds}(0) = \alpha_{\bar{d}d}(0) + \alpha_{\bar{s}s}(0), \quad (23)$$

$$2/\alpha'_{ds} = 1/\alpha'_{\bar{d}d} + 1/\alpha'_{\bar{s}s}. \quad (24)$$

Using the Λ trajectory as input [10],

$$\alpha_{ds} = \alpha_\Lambda = -0.65 + 0.94t, \quad (25)$$

and $\alpha_{\bar{s}s}$ from Eq. (6), one can evaluate the diagonal $\alpha_{\bar{d}d}$ trajectory at small $|t|$ as

$$\alpha_{\bar{d}d}(t) = -1.58 + \alpha'_{\bar{d}d}\,t \quad (26)$$

with $\alpha'_{\bar{d}d} = 1.542$ GeV^{-2}.

The equation for the energy scale parameter $s_{\bar{p}p:\bar{K}K}$ is slightly different from Eq. (7). Now it reads

$$(s_{\bar{p}p:\bar{K}K})^{2[\alpha_{ds}(0)-\frac{1}{2}]} = (s_{\bar{p}p})^{\alpha_{\bar{d}d}(0)} \times (s_{\bar{K}K})^{\alpha_{\bar{s}s}(0)-1}. \quad (27)$$

Using $s_{\bar{K}K} = 1.21$ GeV^2 and $s_{\bar{p}p} = 2.25$ GeV^2, one gets $s_{\bar{p}p:\bar{K}K} = 1.853$ GeV^2.

The spin dependence of the amplitude in Eq. (22) is determined by the form of the $KN\Lambda$ interaction given by the effective Lagrangian

$$\mathcal{L}_{NYK} = -i\bar{N}\,\gamma_5 Y K + \text{h.c.}, \quad (28)$$

where N, Y, and K denote the nucleon, hyperon, and the K meson fields, respectively, and Y stands for Λ, Σ, and so on. This form leads to the following expression of the amplitude $\mathcal{M}$ in Eq. (22):

$$\begin{aligned}\mathcal{M}^{\bar{p}p\to\bar{K}K}_{m_in_i}(s,t) &= \mathcal{N}(s,t)\,[\bar{v}_{n_i}(\not{p}_Y - M_Y)u_{m_i}],\\ \mathcal{N}(s,t) &= \frac{F_\infty(s)}{F(s,t)}, \quad F^2_\infty(s) = s\,M_Y^2/2,\\ F^2(s,t) &= \tfrac{1}{2}\big[\big(s-2M_N^2\big)\big(M_Y^2-t\big)\\ &\quad + 4M_NM_Y\big(M_N^2+M_K^2+t\\ &\quad - \big(M_N^2-M_K^2+t\big)^2 - M_N^2\big(M_Y^2+t\big)\big],\end{aligned} \quad (29)$$

where $p_Y = p_p - p_K$.

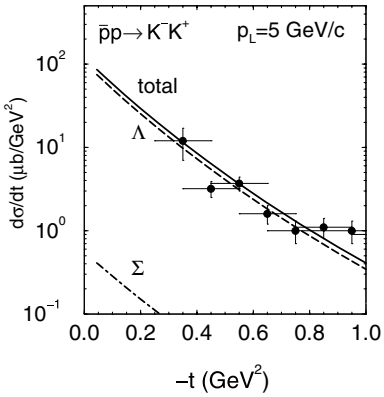

FIG. 10. Differential cross section of the $\bar{p}p \to K^- K^+$ reaction as a function of momentum transfer t at $p_L = 5$ GeV. The contributions from Λ and Σ exchanges are shown by dashed and dot-dashed curves, respectively. The experimental data are taken from Ref. [34].

For the KNY coupling constants we use the average values of the Nijmegen potential [30]: $g_{KNY} = -15.755$ for $Y = \Lambda$ and $g_{KNY} = -4.785$ for $Y = \Sigma^0$.

In case of the $\bar{p}p \to K^- K^+$ reaction, the total amplitude is the coherent sum of the Λ and Σ exchange trajectories, whereas the reaction $\bar{p}p \to \bar{K}^0 K^0$ is dominated by the Σ^+ trajectory. Following Ref. [10] we use

$$\alpha_\Sigma \simeq \alpha_{\Sigma^+} \simeq -0.79 + 0.87t. \tag{30}$$

For simplicity, for the Σ exchange channels we use the same the energy scale parameter as for the Λ exchange, taking into account similarity of the corresponding trajectories and the fact that the contribution of the Σ exchange amplitude is much smaller than the dominant Λ exchange one.

B. Reaction $\bar{p}p \to D\bar{D}$

In this case, the amplitude is defined by Eq. (22) with the substitutions $\Lambda \to \Lambda_c^+ \equiv \Lambda_c$, $\Sigma^0 \to \Sigma_c^+$, $\Sigma^+ \to \Sigma_c^{++}$, $K^+ \to \bar{D}^0$, $K^- \to D^0$, $K^0 \to D^-$, and $\bar{K}^0 \to D^+$ and so on. As before, we assume the validity of SU(4) symmetry, which means that the coupling constants of the DNY_c interaction are chosen to be the same as for the case of the KNY interaction.

The Λ_c trajectory is calculated by using

$$2\alpha_{dc}(0) = \alpha_{\bar{d}d}(0) + \alpha_{\bar{c}c}(0), \tag{31}$$

$$2/\alpha'_{dc} = 1/\alpha'_{\bar{d}d} + 1/\alpha'_{\bar{c}c}, \tag{32}$$

where $\alpha_{\bar{c}c}(t) \equiv \alpha_{J/\psi}(t)$ and $\alpha_{dd}(t)$ are defined by Eqs. (15) and (26), respectively. Thus, for $\alpha_{dc}(t)$ and the energy scale parameter $s_{\bar{p}p:D\bar{D}}$ we have

$$\alpha'_{dc}(0) \simeq -2.09, \quad \alpha'_{dc} \simeq 0.557\,\text{GeV}^{-2}, \tag{33}$$

$$s_{\bar{p}p:D\bar{D}} \simeq 3.59\,\text{GeV}^2. \tag{34}$$

For simplicity, we assume $\alpha_{\Lambda_c^+} \equiv \alpha_{dc} \simeq \alpha_{\Sigma_c^+} \simeq \alpha_{\Sigma_c^{++}}$.

C. Results

1. *Differential cross sections*

The differential cross section of the $\bar{p}p \to \bar{K}^- K^+$ reaction as a function of the momentum transfer $t = (p_p - p_{K^+})^2$ at initial momentum $p_L = 5$ GeV/c together with available experimental data [34] is presented in Fig. 10. The separate contributions from Λ and Σ^0 exchange are shown by dashed and dot-dashed curves, respectively. The solid curve is the coherent sum of these contributions. One can see a dominance of the Λ exchange trajectory in $\bar{p}p \to \bar{K}^- K^+$. This reaction is used to fix the residual factor $C'(t)$ in Eq. (22). We find

$$C'(t) = \frac{0.52}{(1 - t/1.15)^2}; \tag{35}$$

that is, it coincides within ~30% with the residual in $\bar{p}p \to \bar{Y}Y$ reactions [cf. Eq. (16)], which supports the consistency of the model.

In Fig. 11 (left panel), we show our prediction for the differential cross sections of the reactions $\bar{p}p \to K^- K^+$ and $\bar{p}p \to \bar{K}^0 K^0$ as a function of $t_{\max} - t$ at the initial momentum $p_L = 10$ GeV/c. The dependence of the differential cross sections on energy ($\sqrt{s}$) at fixed $t_{\max} - t = 0.2$ GeV^2 is exhibited in Fig. 11 (right panel). At large energies the cross sections behave as $\sim s^{-2.3}$ and $\sim s^{-3.58}$ for the $K^- K^+$ and $\bar{K}^0 K^0$ final states, respectively.

Our prediction for the differential cross sections of $D\bar{D}$ pair production is presented in Fig. 12. The left panel illustrates the dependence on $t_{\max} - t$ at fixed $p_L = 15$ GeV/c. The right panel exhibits the dependence on the excess energy $\Delta s^{1/2}$ at fixed $t_{\max} - t = 0.2$ GeV^2. The ratio of the cross sections with

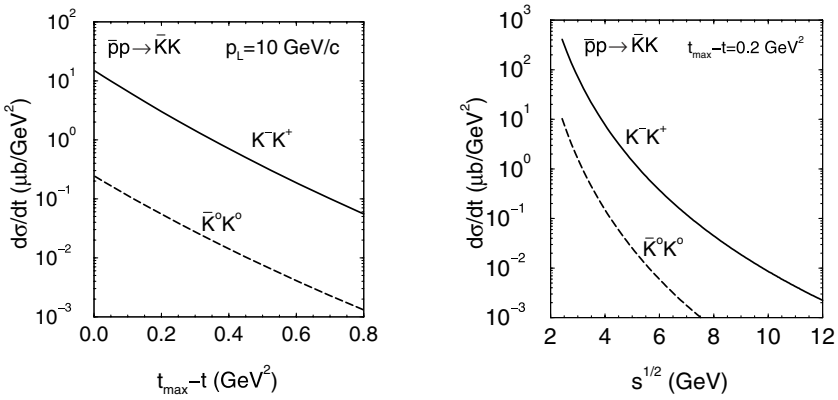

FIG. 11. Left panel: The differential cross sections of the reactions $\bar{p}p \to K^- K^+$ (solid curve) and $\bar{p}p \to \bar{K}^0 K^0$ (dashed curve) as a function of $t_{\max} - t$ at $p_L = 10$ GeV/c. Right panel: The differential cross sections as a function of the energy $\sqrt{s}$ at $t_{\max} - t = 0.2$ GeV^2.

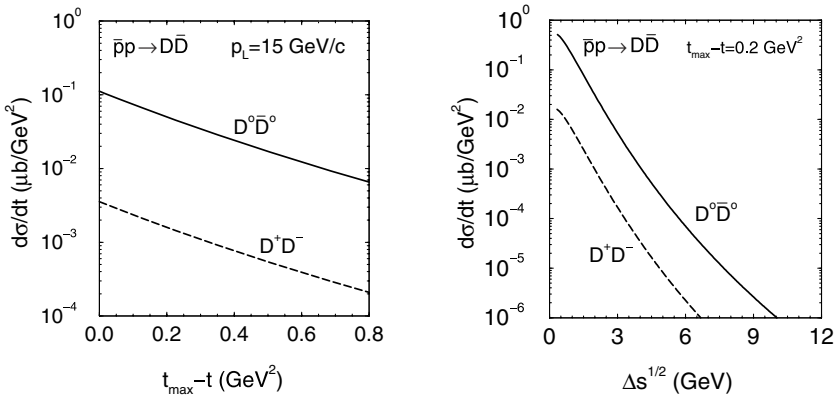

FIG. 12. Left panel: The differential cross sections of the reactions $\bar{p}p \to \bar{D}^0 D^0$ (solid curve) and $\bar{p}p \to D^- D^+$ (dashed curve) as a function of $t_{\max - t}$ at $p_L = 15$ GeV/c. Right panel: The differential cross section as a function of the excess energy $\Delta s^{1/2}$ at $t_{\max} - t = 0.2$ GeV^2.

$D^- D^+$ and $\bar{D}^0 D^0$ final states is close to $(\sqrt{2}\, g_{KN\Sigma}/g_{KN\Lambda})^4 \simeq 0.034$. The cross sections decrease rapidly with energy as $s^{-6.18}$; therefore, the region with small excess energy is more suitable for studying these reactions.

2. Longitudinal asymmetry

In reactions $\bar{p}p \to \bar{K}K$ $(D\bar{D})$ at forward production angle (or $t = t_{\max}$), the spin in the final state is equal to zero. This means that the production amplitude may be expressed as

$$T_{m_i,n_i} \sim B(s)\, \delta_{m_i - n_i}, \tag{36}$$

and therefore the asymmetry in Eq. (14) is $\mathcal{A} = 1$. At finite angles, the spin-orbital interactions becomes important, which leads to an increase of the contribution of $d\sigma^{\rightrightarrows}$ to the total cross section and to a decrease of the asymmetry.

In Fig. 13 we show our prediction for $\bar{p}p \to \bar{K}K$. The left panel exhibits the t dependence at $p_L = 10$ GeV/c, whereas the right panel exhibits the $\sqrt{s}$ dependence at $t_{\max} - t = 0.2$ GeV^2. One can see a decrease of $\mathcal{A}$ with $-t$ and an almost constant value at large $\sqrt{s}$ and fixed $t_{\max} - t$. Some difference in $\mathcal{A}$ for $\bar{K}^0 K^0$ and $K^+ K^-$ final states is explained by the difference of masses of K^0 and $K^\pm$ mesons, which leads to the different relative momenta and to some difference in spin-orbital interactions.

The longitudinal asymmetries for the $\bar{p}p \to D\bar{D}$ reactions are presented in Fig. 14. The left panel demonstrates the t dependence at the initial momentum $p_L = 15$ GeV/c. The right panel shows the dependence on the excess energy at $t_{\max} - t = 0.2$ GeV^2. One can see that the results of the numerical calculation agree with our qualitative consideration. The difference in the asymmetries for $\bar{K}K$ and $D\bar{D}$ final states is mainly due to the difference of masses of kaons and D mesons.

IV. REACTION $\bar{p}p \to \bar{M}M^*$

The reactions $\bar{p}p \to \bar{K}K^*$ and $\bar{p}p \to D\bar{D}^*$ are similar to the reactions with $\bar{K}K$ and $D\bar{D}$ final states, and the corresponding amplitudes are described by the diagrams depicted in Fig. 9, where one of the outgoing pseudoscalar mesons M is replaced by the vector one, M^*, (i.e. $K \to K^*$, $D \to D^*$, etc.). Thus, the invariant amplitude for $\bar{p}p \to \bar{K}K$ reads

$$T^{\bar{p}p\to\bar{K}^- K^{*+}}_{\lambda_f;m_i,n_i} = C'(t)\mathcal{M}^{\bar{p}p\to\bar{K}K}_{\lambda_f;m_i,n_i}(s,t)\frac{g_{K^*N\Lambda} g_{KN\Lambda}}{s_0}\,\Gamma \times \left[\frac{1}{2} - \alpha_{ds}(t)\right]\left(-\frac{s}{s_{\bar{p}p:\bar{K}K^*}}\right)^{\alpha_{ds}(t)-\frac{1}{2}}, \tag{37}$$

where λ_f is the polarization of the outgoing K^* and the other notation has been introduced already in Secs. II and III. The baryon exchange trajectories are the same as in the previous Sec. III, $s_{\bar{p}p:\bar{K}K^*} = s_{\bar{p}p:\bar{K}K}$, and $C'(t)$ is defined in Eq. (35)

The spin-dependent amplitude $\mathcal{M}$ has the following form:

$$\mathcal{M}^{\bar{p}p\to\bar{K}K}_{\lambda_f;m_i n_i}(s,t) = \mathcal{N}(s,t)\,\Gamma^{\mu}_{\lambda_f;m_i n_i}, \tag{38}$$

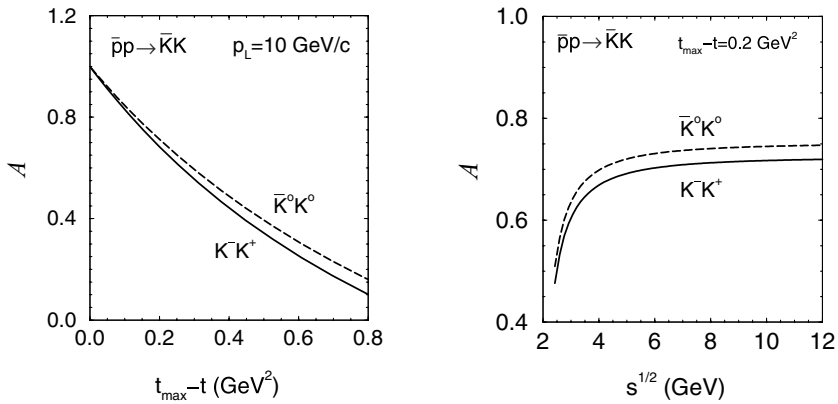

FIG. 13. The longitudinal asymmetry for the reactions $\bar{p}p \to K^- K^+$ (solid curves) and $\bar{p}p \to \bar{K}^0 K^0$ (dashed curves). Left panel: The asymmetry as a function of momentum transfer $t_{\max} - t$ at $p_L = 10$ GeV. Right panel: The asymmetry as a function of the energy $\sqrt{s}$ at $t_{\max} - t = 0.2$ GeV^2.

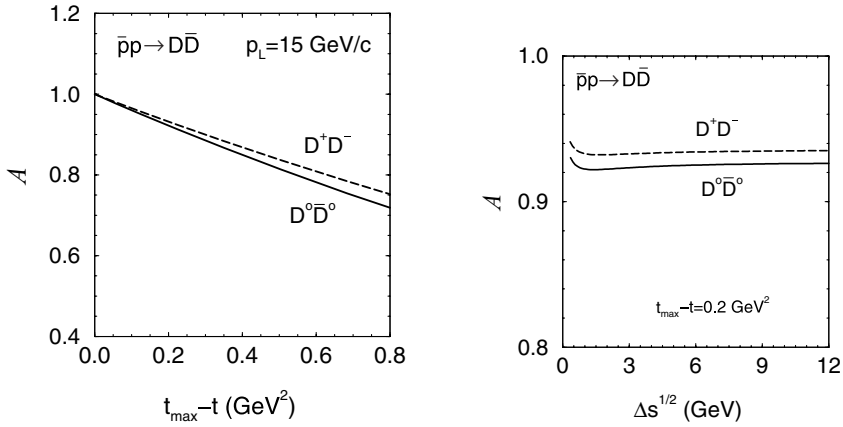

FIG. 14. The longitudinal asymmetry for $\bar{p}p \to D^0\bar{D}^0$ (solid curves) and $\bar{p}p \to D^-D^+$ (dashed curves). Left panel: The asymmetry as a function of momentum transfer $t_{\max} - t$ at $p_L = 15$ GeV. Right panel: The asymmetry as a function of the energy excess $\Delta s^{1/2}$ at $t_{\max} - t = 0.2\ \mathrm{GeV}^2$.

with

$$\Gamma^{\mu}_{\lambda_f;m_i n_i} = \bar{v}_{n_i}\left\{\gamma_5\,(p\!\!\!/ - M_Y)\left[\gamma^{\mu} + \frac{\kappa_{NYK^*}}{2(M_N + M_Y)}(\gamma^{\mu}p\!\!\!/_{K^*} - p\!\!\!/_{K^*}\gamma^{\mu})\right]\right\}u_{m_i}\epsilon^{\mu *}_{\lambda_i}, \tag{39}$$

where $\epsilon^{\mu}_{\lambda_i}$ is the polarization vector of the K^* meson and

$$\mathcal{N}(s,t) = \frac{F_{\infty}(s)}{F(s,t)},$$

with

$$F^2(s,t) = \mathrm{Tr}\left[\Gamma_{\mu}\Gamma_{\nu}{}^{\dagger}\right]\left(-g^{\mu\nu} + \frac{p_V^{\mu}p_V^{\nu}}{M_V^2}\right),$$

$$F_{\infty}^2 = \frac{2sM_Y^2}{M_V^2}\left[M_N^2 + M_V^2 + 6M_N M_V^2 z + M_V^2\left(2M_N^2 + M_V^2\right)z^2\right], \tag{40}$$

where $M_V = M_{K^*}$, $p_V = p_{K^*}$, and $z = \kappa_{VNY}/(M_N + M_Y)$.

In the reaction $\bar{p}p \to K^-K^{*+}$ the total amplitude is the coherent sum of Λ and Σ^0 exchange channels. In the case of $\bar{K}^0K^{*0}$, the amplitude is defined by the Σ^+ exchange trajectory.

The amplitude for the $\bar{K}^*K$ reaction has a similar form:

$$\Gamma^{\mu}_{\lambda_f;m_i n_i} = \bar{v}_{n_i}\left\{\left[\gamma^{\mu} + \frac{\kappa_{NYK^*}}{2(M_N + M_Y)}(\gamma^{\mu}p\!\!\!/_{K^*} - p\!\!\!/_{K^*}\gamma^{\mu})\right](p\!\!\!/ - M_Y)\,\gamma_5\right\}u_{m_i}\epsilon^{\mu *}_{\lambda_i}. \tag{41}$$

The generalization for $D\bar{D}^*$ and $D^*\bar{D}$ final states may be done in a straightforward manner, similarly to that done in the previous sections.

A. Differential cross sections

The differential cross sections of the reactions $\bar{p}p \to \bar{K}K^*$ and $\bar{p}p \to \bar{K}^*K$ are exhibited in Fig. 15. The left panel shows our prediction for the differential cross sections of the reactions $\bar{p}p \to K^-K^{*+}$ and $\bar{p}p \to \bar{K}^0K^{*0}$ as a function of $t_{\max} - t$ at initial momentum $p_L = 10$ GeV/c. The dependence of the differential cross sections on energy $\sqrt{s}$ at fixed $t_{\max} - t = 0.2\ \mathrm{GeV}^2$ is presented in the right panel. At large energies the cross sections behave similarly to the cross sections of the $\bar{p}p \to \bar{K}K$ reactions.

Our prediction for the differential cross sections of the $D\bar{D}^*$ pair production is presented in Fig. 16. The left panel illustrates the dependence on $t_{\max} - t$ at fixed $p_L = 15$ GeV/c. The right panel exhibits the dependence on the energy excess $\Delta s^{1/2}$ at fixed $t_{\max} - t = 0.2\ \mathrm{GeV}^2$. The ratio of the cross sections with D^-D^{*+} and $\bar{D}^0D^0$ final states is defined by the coupling

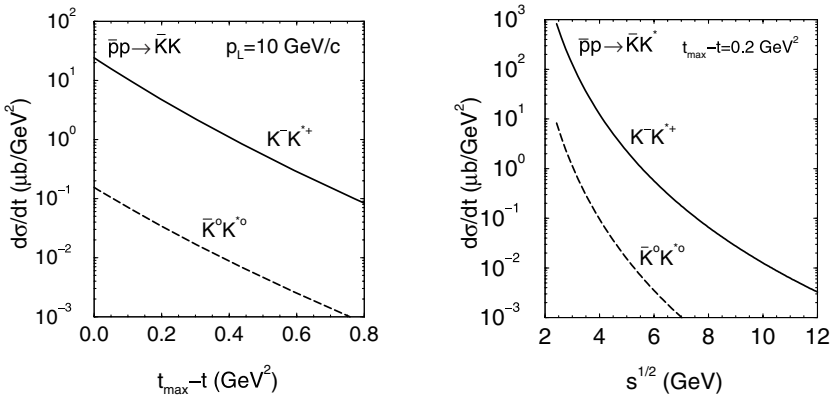

FIG. 15. Left panel: The differential cross sections of the $\bar{p}p \to K^-K^{*+}$ (solid curve) and $\bar{p}p \to \bar{K}^0K$ (dashed curve) reactions as a function of $t_{\max} - t$ at $p_L = 10$ GeV/c. Right panel: The differential cross sections as a function of the energy $\sqrt{s}$ at $t_{\max} - t = 0.2\ \mathrm{GeV}^2$.

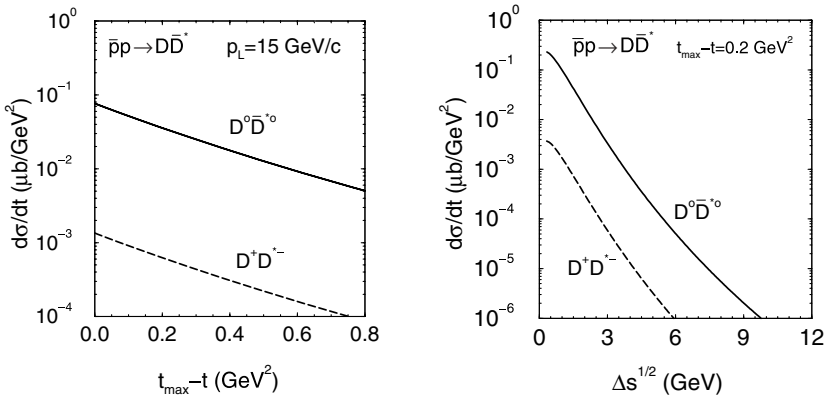

FIG. 16. Left panel: The differential cross sections of the $\bar{p}p \to \bar{D}^0 D^*$ (solid curve) and $\bar{p}p \to D^- D^{*+}$ (dashed curve) reactions as a function of $t_{\max -t}$ at $p_L = 15$ GeV/c. Right panel: The differential cross section as a function of the energy excess $\Delta s^{1/2}$ at $t_{\max} - t = 0.2$ GeV^2.

constants in $KN\Sigma$, $K^*N\Sigma$ and $KN\Lambda$, $K^*N\Lambda$ interactions and is close to 0.03. The cross sections decrease with energy similarly to the $\bar{p}p \to D\bar{D}$ reactions, and therefore the region with small excess energy is more suitable for studying these reactions.

B. Longitudinal asymmetry

Let us consider first the case of the forward production angle (or $t = t_{\max}$) in $\bar{p}p \to \bar{K}K^*$ ($D\bar{D}^*$) reactions with pure vector coupling in $V^*N\Sigma (V = K^*,\ D^*)$. For energies, where $\mathbf{p}_V \simeq \mathbf{p}_p$, the amplitude has the form

$$T_{\lambda_i;m_i,n_i} \sim R(s)\left(A\,\delta_{m_i n_i} + B\ \delta_{-m_i n_i}\right)\delta_{\lambda_i \lambda_V}, \qquad (42)$$

where λ_V is the polarization of the outgoing vector meson, $\lambda_i = m_i + n_i$, and

$$A \simeq \sqrt{2}, \quad B \simeq \frac{M_N}{M_V}, \qquad (43)$$

where M_V is the mass of the vector meson. This results in

$$\mathcal{A} = \frac{M_N^2 - 2M_V^2}{M_N^2 + 2M_V^2}. \qquad (44)$$

Thus, for the $\bar{K}K^*$ final state, where $M_V \sim M_N$, the asymmetry has values $\mathcal{A} \simeq -0.3$ and increases at finite production angles because of the spin-orbital interaction. For the $\bar{p}p \to D\bar{D}^*$ reaction, the asymmetry is much smaller, $\mathcal{A} \simeq -0.8$, and it also increases with the production angle. The finite tensor coupling changes these predictions, especially in the charm sector with large M_V.

In Fig. 17 we show our prediction for the $\bar{p}p \to \bar{K}K^*$ reactions. The left panel exhibits the t dependence at $p_L = 10$ GeV/c, whereas the right panel depicts the $\sqrt{s}$ dependence at $t_{\max} - t = 0.2$ GeV^2. One can see an increase of the asymmetry with $-t$ and its almost constant value at large $\sqrt{s}$ and fixed $t_{\max} - t$. The difference in $\mathcal{A}$ for $\bar{K}^0 K^{*0}$ and $K^+ K^{*-}$ final states is mainly due to the difference in tensor couplings in $K^*N\Sigma$ and $K^*N\Lambda$ interactions. For completeness, we also show the result for a calculation without tensor couplings. At zero production angle the asymmetry is close to our qualitative estimate.

The longitudinal asymmetries for $\bar{p}p \to D\bar{D}^*$ reaction are presented in Fig. 18. The left panel displays the t dependence at initial momentum $p_L = 15$ GeV/c. The right panel shows the dependence on the energy excess at $t_{\max} - t = 0.2$ GeV^2. We also show results for a calculation with pure vector couplings. At zero production angle the asymmetry (left panel) coincides with our qualitative estimate [cf. Eq. (44)]. The effect of the tensor interaction is rather large. One can see a big difference between $D^0 D^{*0}$ and $D^- D^{*+}$ final states because of the difference in the corresponding tensor couplings. Numerically, result for the $D^- D^{*+}$ final state is close to a calculation with zero tensor coupling.

V. SUMMARY

In summary, we have analyzed the open charm production in the exclusive binary reactions $\bar{p}p \to \bar{Y}_c Y_c$, $\bar{p}p \to D\bar{D}$, and $\bar{p}p \to D\bar{D}^*$ at small momentum transfer. Our consideration

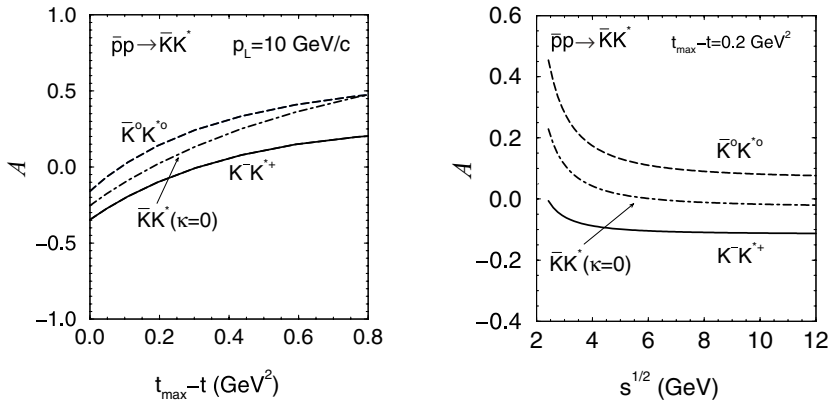

FIG. 17. The longitudinal asymmetry for the reactions $\bar{p}p \to K^- K^{*+}$ (solid curves) and $\bar{p}p \to \bar{K}^0 K^{*0}$ (dashed curves). The dot-dashed curves correspond to the calculation with zero tensor coupling constant. Left panel: The asymmetry as a function of momentum transfer $t_{\max} - t$ at $p_L = 10$ GeV. Right panel: The asymmetry as a function of the energy $\sqrt{s}$ at $t_{\max} - t = 0.2$ GeV^2.

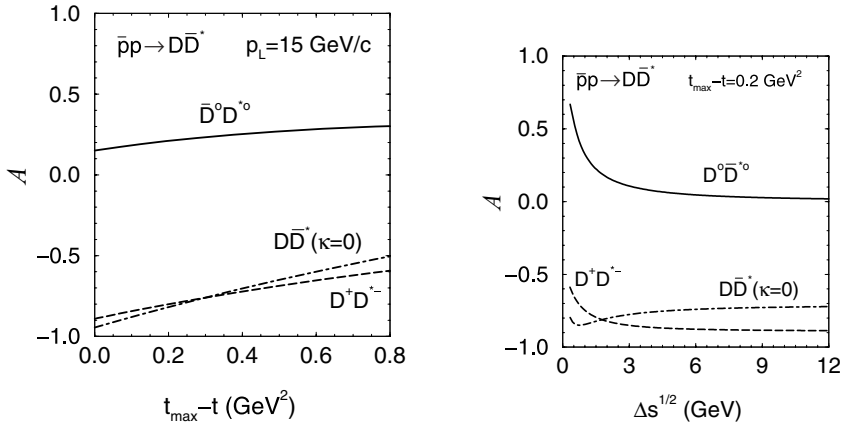

FIG. 18. The longitudinal asymmetry for the reactions $\bar{p}p \to D^0\bar{D}^{*0}$ (solid curves) and $\bar{p}p \to D^-D^+$ (dashed curves). The dot-dashed curves correspond to the calculation with zero tensor coupling constant. Left panel: The asymmetry as a function of momentum transfer $t_{\max} - t$ at $p_L = 15$ GeV. Right panel: The asymmetry as a function of the excess energy $\Delta\sqrt{s}$ at $t_{\max} - t = 0.2$ GeV^2

is based on a modified Regge-type model, motivated by quark-gluon string dynamics. The most important parameters of the model are the effective charmed meson and baryon exchange trajectories and the energy scale parameters. They are found from a consistent approach based on the topological decomposition and factorization of the corresponding planar quark diagrams. The coupling constants are taken to be the same as in corresponding strangeness production reactions, under the assumption of SU(4) symmetry. Unknown residual functions are found from the comparison of the calculation of $\bar{p}p \to \bar{\Lambda}\Lambda\,(\bar{\Lambda}\Sigma)$ and $\bar{p}p \to \bar{K}K$ reactions with available (although old) experimental data. As a result, we obtained the absolute value of the corresponding cross sections in the energy range of future FAIR experiments.

For the first time we made predictions for the longitudinal asymmetry, which is quite different in different processes with nontrivial t and s dependencies. In each case we presented an analytical estimate for the forward production with the aim at understanding the physics of the asymmetry.

Our calculations of cross sections and longitudinal asymmetries in the exclusive reactions $\bar{p}p \to \bar{Y}Y$, $\bar{p}p \to \bar{K}K$, and $\bar{p}p \to \bar{K}K^*$ are also of independent interest for forthcoming experiments at FAIR as a first prediction of the open strangeness production in peripheral reactions in this energy region. Our consideration may serve as a first step toward more involved reaction mechanisms and extensions to pp collisions.

ACKNOWLEDGMENTS

One of the authors (A.I.T.) appreciates the warm hospitality in Forschungszentrum Dresden-Rossendorf. This work was supported by BMBF Grant No. 06DR136 and GSI-FE.

[1] V. Friese, Nucl. Phys. **A774**, 377 (2006); current information on the GSI-FAIR project may be found at http://www.gsi.de/fair.
[2] See http://www.gsi.de/fair/experiments/hesr-panda/pandagsi.html.
[3] See http://niham.nipne.ro/old/index.php?id=49.
[4] V. Barone *et al.* (PAX Collaboration), arXiv:hep-ex/0505054.
[5] P. Nason, S. Dawson, and R. K. Ellis, Nucl. Phys. **B327**, 49 (1989) [Erratum-*ibid.* **B335**, 260 (1990)].
[6] R. Vogt, Eur. Phys. J. ST **155**, 213 (2008).
[7] T. Kneesch, B. A. Kniehl, G. Kramer, and I. Schienbein, Nucl. Phys. **B799**, 34 (2008).
[8] D. de Florian and W. Vogelsang, Phys. Rev. D **71**, 114004 (2005); **72**, 014014 (2005).
[9] J. Riedl, A. Schäfer, and M. Stratmann, Eur. Phys. J. C **52**, 987 (2007).
[10] J. K. Storrow, Phys. Rep. **103**, 317 (1984).
[11] M. Saleem and M. Ali, Lett. Nuovo Cimento **32**, 425 (1981).
[12] G. Plaut, Nucl. Phys. **B35**, 221 (1971).
[13] B. Sadoulet, Nucl. Phys. **B53**, 135 (1973).
[14] L. Burakovsky, T. Goldman, and L. P. Horwitz, Phys. Rev. D **56**, 7124 (1997).
[15] M. M. Brisudova, L. Burakovsky, and T. Goldman, Phys. Rev. D **61**, 054013 (2000).
[16] A. B. Kaidalov, Z. Phys. C **12**, 63 (1982).
[17] K. G. Boreskov and A. B. Kaidalov, Sov. J. Nucl. Phys. **37**, 100 (1983); [Yad. Fiz. **37**, 174 (1983)].
[18] A. B. Kaidalov and O. I. Piskunova, Sov. J. Nucl. Phys. **43**, 994 (1986); [Yad. Fiz. **43**, 1545 (1986)].
[19] F. E. Low, Phys. Rev. D **12**, 163 (1975).
[20] S. Nussinov, Phys. Rev. D **14**, 246 (1976).
[21] A. I. Titov, B. Kämpfer, and B. L. Reznik, Eur. Phys. J. A **7**, 543 (2000).
[22] M. Guidal, J. M. Laget, and M. Vanderhaeghen, Nucl. Phys. **A627**, 645 (1997).
[23] G. I. Lykasov and M. N. Sergeenko, Z. Phys. C **56**, 697 (1992).
[24] G. G. Arakelian and P. E. Volkovitsky, Z. Phys. A **353**, 87 (1995).
[25] E. Tomasi-Gustafsson and M. P. Rekalo, Phys. Rev. D **69**, 094015 (2004).
[26] W. Cassing, L. A. Kondratyuk, G. I. Lykasov, and M. V. Rzjanin, Phys. Lett. **B513**, 1 (2001).
[27] O. Linnyk, E. L. Bratkovskaya, W. Cassing, and H. Stöcker, Nucl. Phys. **A786**, 183 (2007).
[28] A. Sibirtsev, K. Tsushima, and A. W. Thomas, Phys. Rev. C **63**, 044906 (2001).

[29] W. Cassing, E. L. Bratkovskaya, and A. Sibirtsev, Nucl. Phys. **A691**, 753 (2001); B. Kämpfer, O. P. Pavlenko, and K. Gallmeister, Phys. Lett. **B419**, 412 (1998).
[30] V. G. J. Stoks and T. A. Rijken, Phys. Rev. C **59**, 3009 (1999).
[31] H. Becker *et al*. (CERN-Munich Collaboration), Nucl. Phys. **B141**, 48 (1978).
[32] F. E. Close, *An Introduction to Quarks and Partons* (Academic Press, London, New York, San Francisco, 1979).
[33] M. Fabre de la Ripelle and Yu. A. Simonov, Annals Phys. **212**, 235 (1991).
[34] A. Eide *et al*., Nucl. Phys. **B60**, 173 (1973).